Effect of Copper Dopants on Visible-Light-Driven Photocatalytic Activity of BiFeO$_3$ Photocatalysts

Buagun Samran[1], Pacharee Krongkitsiri[2], and Saranyoo Chaiwichian[2]

1. Division of Physics, Faculty of Science, Nakhon Phanom University, Thailand

2. Department of Science and Mathematics, Faculty of Industry and Technology, Rajamangala University of Technology Isan, Thailand

Abstract: In this study, visible-light- induced BiFeO$_3$ nanoparticles have been successfully synthesized by a co-precipitation method with different copper (Cu) concentrations varying from 0.5-5.0 mol%. The physicochemical properties of the as-synthesized samples were characterized using X-ray diffraction (XRD), scanning electron microscopy (SEM), transmission electron microscopy (TEM), Brunauer-Emmett-Teller (BET)-specific surface area, X-ray photoelectron spectroscopy (XPS), Photoluminescence (PL) and UV-vis diffuse reflectance spectroscopy (UV-vis DRS) techniques. It was shown that the doping of Cu2+ had no effect on the phase structure of BiFeO$_3$ but displays a considerable role on the photocatalytic activity. Results showed that the doped Cu into BiFeO3 could significantly enhance the photocatalytic activity of BiFeO3 for methyl orange (MO) degradation under visible light irradiation, which was attributed to Cu ions acting as electron traps and inhibited quick recombination of photogenerated charge carriers. The photocatalytic results demonstrated that Cu-BiFeO3 exhibited higher photodegradation than pure BiFeO$_3$. Moreover, the stability and long-time reusability of the sample was also examined by five recycles for the photodegradation testing of MO under visible light irradiation.

Key words: BiFeO$_3$, Nanoparticles, Co-precipitation method, Methyl orange, Photocatalytic activity

1. Introduction

Heterogeneous photocatalysis has been regarded as a clean technology. It has gained lots popularity for the degradation of organic pollutants from papermaking and textile industries as well as environmental treatment in the past decades [1-4]. The advantages of heterogeneous photocatalysis include quick chemical reaction and its environmentally friendly nature. In recent years, TiO$_2$ has extensively been used as a photocatalysts in organic pollutants degradation and water splitting due to its nontoxicity, good stability and low cost [5, 6]. However, the limitations of TiO$_2$ are its large band gap energy of 3.2 eV and the condition that it can only be utilizable under ultraviolet light, which

accounts for approximately 4% of the solar energy [5, 6]. Therefore, it is extremely necessary to seek the semiconductor photocatalysts with high activity under visible light. Bismuth ferrite (BiFeO$_3$) is an inorganic chemical compound with ferroelectric propeerties and antiferromagnetic ordering. It has a rhombohedrally distorted perovskite structure [7]. In addition, BiFeO$_3$ has also earned a great deal of attention for its practical applications as highly efficient visible-light photocatalyst for organic pollutants and environmental remediation. This is due to its narrow band gap energy of 2.1-2.2 eV and high chemical stability in aqueous solution [8-11]. However, the quick recombination of electrons and holes in pristine BiFeO$_3$ is a serious problem, leading to a decrease of photocatalytic activity. To solve this problem, various researchers have focused on the improvement of photocatalytic performance with doping transition metal ions such as

Corresponding author: Saranyoo Chaiwichian, Ph.D., areas/interests: advanced materials & nanotechnology. E-mail: saranyou530531117@gmail.com.

Gd, Ag, Sm, Pt, La, Ba, Fe and so on [11-16]. Doping with transition metal ions into semiconductor photocatalyst surface have been employed to act as electron traps to hinder the recombination of photoinduced charge carriers and increased the lifetime of charge carriers. Therefore, Cu-doped $BiFeO_3$ is an interesting research area for its photocatalytic applications. However, so far as we know, there has been few report on Cu-doped $BiFeO_3$ and its photocatalytic properties.

In this study, the Cu-doped $BiFeO_3$ was synthesized via a co-precipitation method with different copper (Cu) concentrations. The photocatalytic activities of all samples were examined by the photodegradation of methyl orange (MO) in aqueous solution under visible light irradiation.

2. Experimental Section

2.1 Preparation of Photocatalysts

2.1.1 Preparation of BiFeO₃

The chemical co-precipitation method was employed to prepare pure $BiFeO_3$ nanoparticles. In a typical synthesis, 0.1 M of $Bi(NO_3)_3•5H_2O$ was dissolved in 2.5 M of HNO_3 solution, while 0.1 M of $Fe(NO_3)_3•9H_2O$ was dissolved in 50 mL of deionized water. Then, both solutions were mixed together under constant stirring for 30 min at room temperature. The obtained mixture was adjusted to a pH of 10 using 6 M of NaOH solution, and then the solution was continuously stirred for 24 h to complete the ferritization process. Finally, the precipitates of $BiFeO_3$ were washed with deionized water and ethanol several times until pH of 7 was attained. It was then dried at 80°C for 24. All precipitates of $BiFeO_3$ were calcined at the temperature of 600°C for 3 h.

2.1.2 Preparation of Cu-BiFeO₃

The $Bi(NO_3)_3•5H_2O$ and $Fe(NO_3)_3•9H_2O$ was used as a precursor for preparing Cu-$BiFeO_3$ nanoparticles. Firstly, $Bi(NO_3)_3•5H_2O$ (0.1 M) was dissolved in HNO_3 solution (2.5 M), and $Fe(NO_3)_3•9H_2O$ (0.1 M) was dissolved in deionized water (50 ml). Then, the obtained solutions were mixed together under continuously magnetic stirring until the solution was homogeneous. The concentrated NaOH (6 M) was then added dropwise to the solution to stabilize the pH at 10 and followed by introducing $Cu(NO_3)_2•3H_2O$ with concentrations varying from 0.5-5.0 mol%. The precipitates were separated by the centrifugation and washed with deionized water and ethanol several times. Finally, the Cu-$BiFeO_3$ particles were dried at the temperature of 80°C for 24 h and calcined at 600°C for 3 h.

2.2 Characterization of Photocatalysts

X-ray diffraction (XRD, Philips X'Pert MPD) with Cu Kα irradiation (λ = 1.5418 nm) in the 2θ ranging from 10° to 80° was used to investigate phase and composition. The as-obtained morphologies were examined using scanning electron microscopy (SEM, JEOL JSM-6335F) technique. Transmission electron microscopy (TEM, JEOL JEM-2010) was employed to find the actual size and microstructure. The Brunauer-Emmett-Teller (BET) surface area was calculated using nitrogen adsorption-desorption isotherm measurements at 80°C (Autosorb 1 MP, Quantachrome). The elemental compositions of products were analyzed by X-ray photoelectron spectroscopy (XPS, AXIS ULTRA^{DLD}, Kratos analytical, Manchester UK). The instrument equipped with X-ray hybrid mode 700×300 μm spot areas with a monochromatic Al K_α radiation at 1.4 keV. The binding energies of the adventitious carbon (C 1s) line at 284.6 eV were used for calibration, and the positions of other peaks were corrected according to the position of the C 1s signal. UV-vis diffuse reflection spectroscopy (UV-vis 3600, Shimadzu) with an integrating sphere attachment (ISR-3100, Shimadzu) was used to observe the optical properties of all samples. Photoluminescence (PL) was tested using AvaSpec-2048TEC-USB2-2 spectrophotometer excited by LED (Oceans optics, LLS-345) as a light source with a wavelength of 345 nm.

2.3 Photocatalytic Experiments

The photocatalytic activities of products were studied by degrading methyl orange (MO) in aqueous solution under visible light irradiation with a 50 W halogen lamp (Essential MR, Philips (Thailand)) as a light source (a cutoff filter of 400 nm). 2×10^{-5} M was used as an initial concentration of organic dye. The catalyst powder of 0.1 g was added into 100 ml of MO solution under magnetic stirring and dispersed in aqueous solution. The solution was then kept in dark for 1 h to ensure an adsorption-desorption equilibrium of the organic dye on the catalyst surface was reached before the light irradiation. Then the reaction system was irradiated with visible light. The suspension of 3 mL was taken every 15 min together with centrifuging at 5000 rpm for 10 min to separate photocatalyst particles. The absorbance of MO (554 nm) solution was detected by a UV-vis spectrophotometer (Shimadzu UV-1800).

3. Results and Discussion

3.1 XRD and BET Analyses

The phase and compositions of as-prepared samples were investigated by X-ray diffraction (XRD) technique, as shown in Fig. 1a. The diffraction peaks of $BiFeO_3$ can be identified as a single rhombohedral phase which agrees with the JCPDS files no. 72-2035. Meanwhile, the Cu-$BiFeO_3$ nanoparticles show similar diffraction peaks to the pure $BiFeO_3$ sample and no other peaks or impurities are detected, confirming the high purity phases of all the samples. Moreover, it is also found that the presence of Cu^{2+} does not change the phase structure of $BiFeO_3$, and Cu peaks have not appeared, may be due to very low concentration of Cu into $BiFeO_3$. To study the details of the crystal structure of Cu-$BiFeO_3$, we enlarge the XRD peaks at $2\theta = 31.89°$ and $32.18°$ of the samples, as shown in Fig. 1b. The results show that the positions of rhombohedral (110) and (-110) planes shift toward higher 2θ values. This phenomenon may be attributed to the lattice
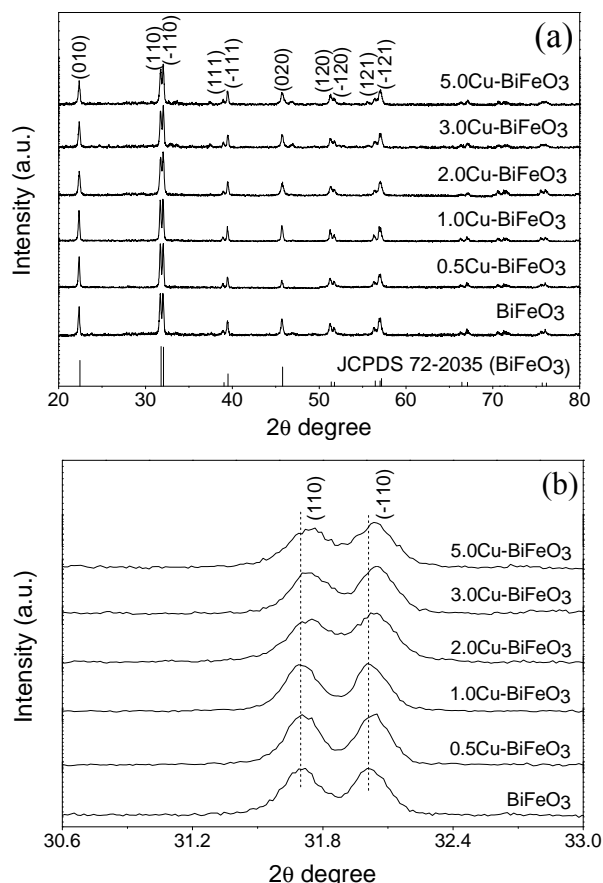
Fig. 1 XRD patterns of pure BiFeO₃ and Cu-BiFeO₃ nanoparticles with different Cu concentrations varying from 0.5-5.0 mol%; (b) the enlarged XRD patterns at 2θ = 30.6° to 33.0°.

extension owing to the petty portion of Cu atom incorporation. This indicat that Cu may have a definite effect on the (110) and (-110) planes of $BiFeO_3$, considering that the ionic radius of Cu^{2+} (0.73 Å) is much smaller than that of Bi^{3+} (1.03 Å) but close to that of Fe^{3+} (0.64 Å). Therefore, the lattice extension is much more probable to be resulting from the substitution of Fe^{3+} (0.64 Å) with Cu^{2+} (0.73 Å) ions. The specific surface area of $BiFeO_3$ and 1.0 mol% Cu-$BiFeO_3$ samples was measured by nitrogen adsorption BET method. The BET surface area of $BiFeO_3$ is estimated to be 3.83 m^2/g, and the specific surface area of 1.0 mol% Cu-$BiFeO_3$ is 10.25 m^2/g. The BET results show that the Cu doping into the $BiFeO_3$ resulted in an increase of specific surface area, which may arise from the substitution of Cu^{2+} into Fe^{3+} in $BiFeO_3$ lattice. Therefore, the increase of the specific

surface area make it possible to help more adsorption on active sites and is the key factor in enhancing photocatalytic efficiency for the degradation of organic pollutants under visible light irradiation. Moreover, increase of phohtocatalytic activity is also dependent on other factors, such as crystallinity, morphology, pH, light intensity and so on [17-19].

3.2 SEM-EDS Analysis

The morphology of all the samples was analysed using scanning electron microscopy (SEM) technique, as shown in Fig. 2. The SEM image of pure BiFeO₃ is an irregular structure with an average size of ranging from 60-100 nm, as illustrated in Fig. 2a. Meanwhile, the SEM images of doping Cu into BiFeO₃ were similar to the BiFeO₃ (Fig. 2b). To further highlight the presence of the Cu ions in Cu-BiFeO₃ nanoparticles and elemental compositions of Cu-BiFeO₃, the EDS technique was used. The results indicate that Cu-BiFeO₃ composes of Cu, Bi, Fe and O elements, as shown in Fig. 2c.

3.3 TEM Analysis

The TEM technique was used to investigate more information of morphology of 1.0 mol% Cu-BiFeO₃ nanoparticles, as shown in Fig. 3. Fig. 3a shows the TEM image of 1.0 mol% Cu-BiFeO₃. It can be clearly seen that the morphology of the 1.0 mol% Cu-BiFeO₃ nanoparticles has irregular particles with a diameter size of approximately 100 nm. The lattice fringe of the sample is approximately 0.2813 nm and matches the (110) crystallographic plane of rhombohedra Cu-BiFeO₃, as illustrated in Fig. 3b.

3.4 XPS Analysis

The XPS technique was used to determine the chemical composition and oxidation states of Bi, Fe, O and Cu elements in the 1.0 mol% Cu-BiFeO₃ nanoparticles, as shown in Fig. 4. Fig. 4a-d shows the XPS spectra of Bi 4f, Fe 2p, O 1s and Cu 2p orbitals, respectively. From Fig. 4a, the Bi 4f displays two peaks
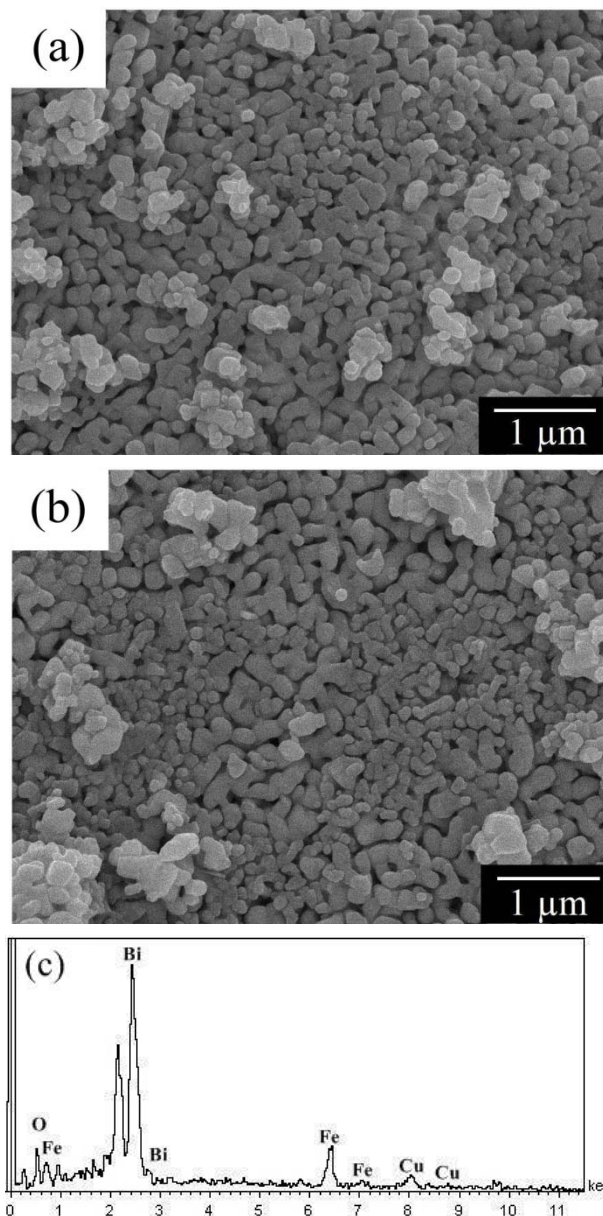
Fig. 2   SEM images of (a) pure BiFeO₃; (b) 1.0 mol% Cu-BiFeO₃ nanoparticles and (c) EDS spectrum of 1.0 mol% Cu-BiFeO₃ nanoparticles.
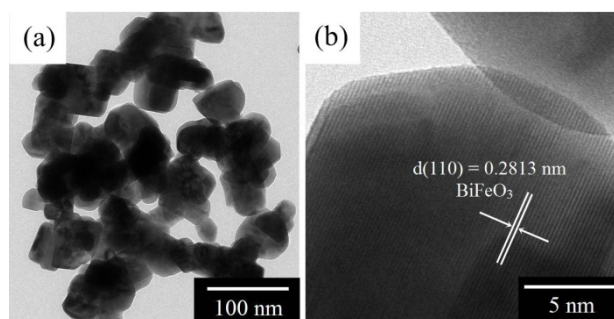
Fig. 3   TEM photographs of (a) 1.0 mol% Cu-BiFeO₃ nanoparticles; (b) lattice fringe of 1.0 mol% Cu-BiFeO₃ nanoparticles.
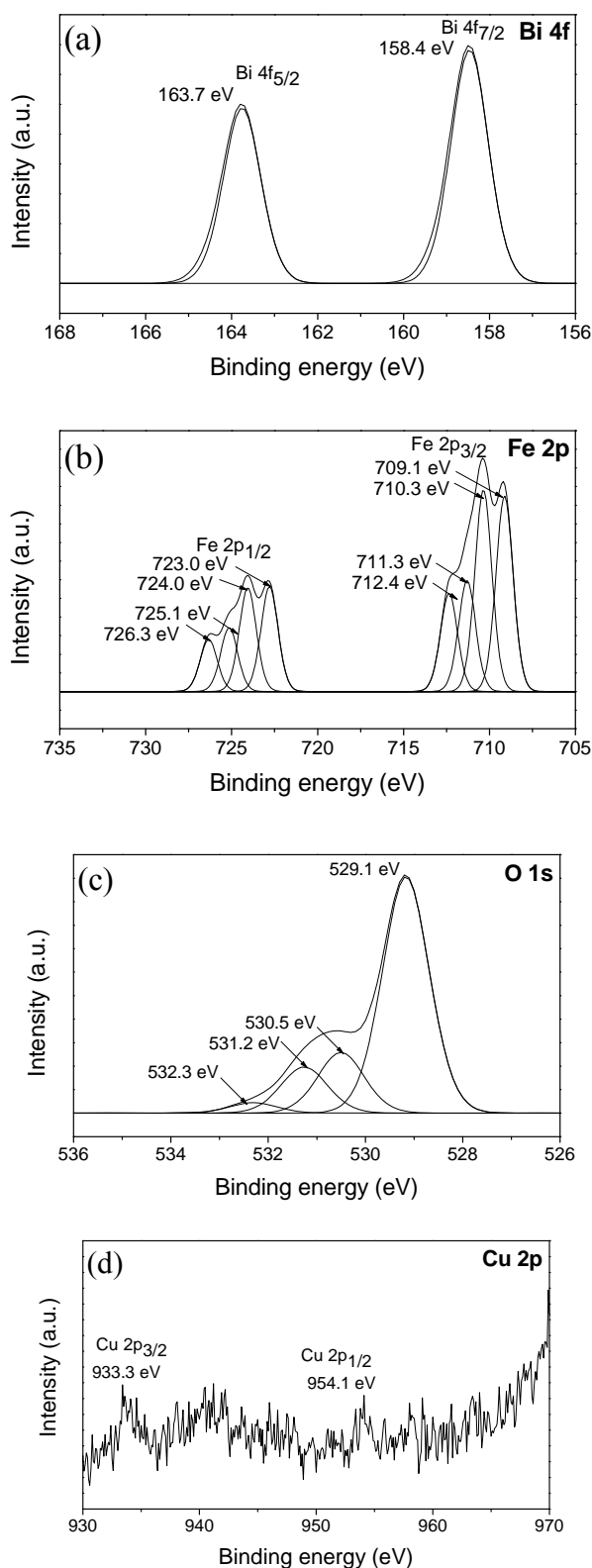
Fig. 4   XPS spectra of (a) Bi 4f; (b) Fe 2p; (c) O 1s and (d) Cu 2p orbitals of pure BiFeO₃ and 1.0 mol% Cu-BiFeO₃ nanoparticles.

with binding energies of 158.4 eV and 164.7 eV, which correspond to the Bi $4f_{7/2}$ and Bi $4f_{5/2}$, respectively, and can be assigned to a Bi^{3+} [20, 21]. In Fig. 4b, the binding energies of Fe 2p at 709.1 and 723.0 eV correspond to the Fe $2p_{3/2}$ and Fe $2p_{1/2}$ are attributed to Fe^{2+}. The peaks appear at binding energies of 710.3-711.3 eV and 724.0-725.1 eV corresponding to the Fe $2p_{3/2}$ and Fe $2p_{1/2}$, which can be considered as the characteristic peaks of Fe^{3+} [22-24]. Moreover, the binding energies of 712.4 eV for Fe $2p_{3/2}$ and 726.3 eV for Fe $2p_{1/2}$ can be assignable to Fe^{3+} in FeOOH [24-26]. This observation may be attributed to oxyhydroxide from ethanol during sample preparation. The O 1s peaks are deconvoluted into four main peaks in the range of 529.1-532.3 eV, as shown in Fig. 4c. The characteristic peaks at binding energies of 529.1 eV and 530.5 eV can be assigned to the O^{2-} in the lattice oxygen in BiFeO₃. The binding energies at 531.2 eV and 532.3 eV may come from the hydroxyl groups and oxygen species in chemisorbed water, respectively [27, 28]. Fig. 4d shows the XPS spectra of Cu 2p. The Cu $2p_{3/2}$ and Cu $2p_{1/2}$ peaks are located at 933.3 eV and 954.1 eV, respectively, which can be confirmed to be due to the presence of Cu^{2+} in the Cu-BiFeO₃ nanoparticles [29-31].

3.5 UV-vis DRS Analysis

The UV-vis diffuse reflectance spectra (UV-vis DRS) was employed to measure the optical properties of BiFeO₃ and 1.0 mol% Cu-BiFeO₃ nanoparticles. As shown in Fig. 5, the absorption of BiFeO₃ and 1.0 mol% Cu- BiFeO₃ nanoparticles is in the visible light region. The band gap energy of all samples can be calculated by the following equation; $E_g = 1241/\lambda$, where E_g is the band gap energy and λ is the wavelength of light. The obtained results reveal that the band gap energies of BiFeO₃ and 1.0 mol% Cu-BiFeO₃ nanoparticles are to be 2.14 eV and 2.12 eV, respectively. It can be seen that the band gap energy of Cu-BiFeO₃ nanoparticles is lower than the pure BiFeO₃. This is important, as it shows that the 1.0 mol%

Cu-BiFeO$_3$ nanoparticles can be photoexcited to create more electron-hole pairs under visible light, which lead to an enhanced photocatalytic performance.

3.6 Photocatalytic Activity Testing

The photocatalytic activities of pure BiFeO$_3$ and Cu-BiFeO$_3$ nanoparticles with different Cu concentrations were carried out by the photodegradation of MO aqueous solution under visible light as shown in Fig. 6a. The MO photolysis test without any photocatalyst is low. In the presence of photocatalysts, the as-prepared Cu-BiFeO$_3$ nanoparticles show higher photodegradation of MO aqueous solution under visible light than that of pure BiFeO$_3$. Specifically, the Cu-BiFeO$_3$ sample with 1.0 mol% of Cu doped exhibits the highest photoactivity for degrading MO aqueous solution in comparison with other samples, and reach up to 67% within 120 min. Moreover, lower or higher concentrations of Cu will lead to a decline the photocatalytic efficiency. The increase of photoactivity in the case of 1.0 mol% Cu-BiFeO$_3$ may be due to Cu ions acting as electron traps, which turns to facilitate the separation of photogenerated electron-hole pairs and reduce the recombination of photoinduced charge carriers. To test the stability of 1.0 mol% Cu-BiFeO$_3$ nanoparticle for it practical application, recycling runs in the photodegradation of MO aqueous solution under visible light irradiation were carried out. As shown in Fig. 6b, the 1.0 mol% Cu-BiFeO$_3$ nanoparticle exhibits an excellent stability under repeated use. After five runs the degradation of MO aqueous solution under visible light irradiation is only decreased of approximately 7%, indicating that the reusability and less photocorrosion during the photocatalysis processes did not show any significant loss of photoactivity. This is an important for wastewater remedy.

3.7 Photocatalytic Mechanism

To study more information in the photocatalytic
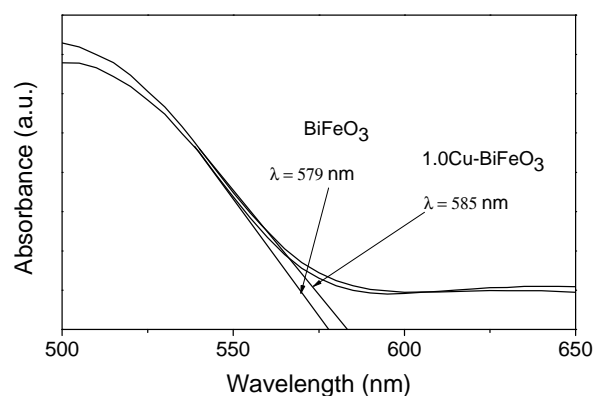
Fig. 5 UV-vis DRS patterns of pure BiFeO$_3$ and 1.0 mol% Cu-BiFeO$_3$ nanoparticles.
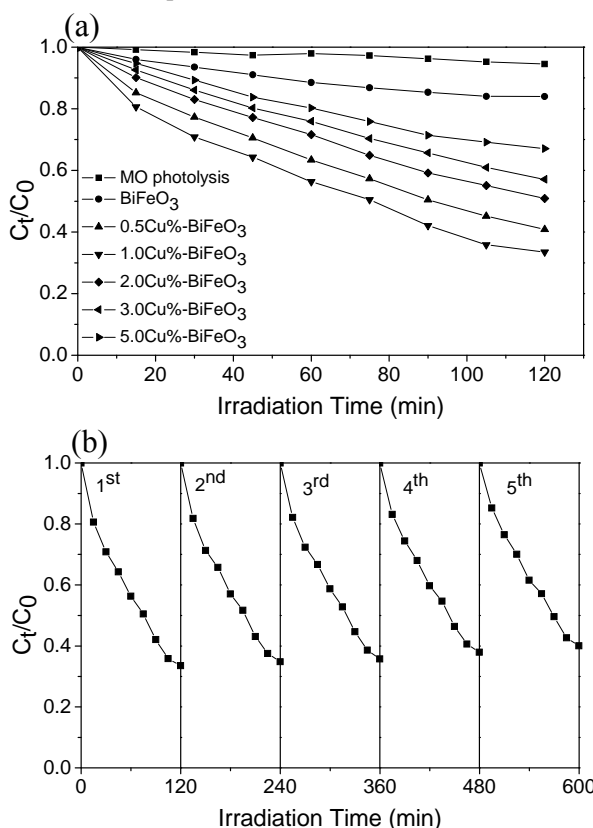
Fig. 6 (a) Photodegradation of MO under visible light irradiation; (b) Recycling runs of 1.0 mol% Cu-BiFeO$_3$ nanoparticles.

mechanism of pure BiFeO$_3$ and 1.0 mol% Cu-BiFeO$_3$ nanoparticles, the trapping experiments were applied to determine the major active species during the photodegradation process. As shown in Fig. 7, 2 mM of benzoquinone (BQ, a superoxide radicals ($O_2^{\bullet-}$) or (e^-) scavenger), isopropanol (IPA, a hydroxyl radical ($OH^{\bullet}$) scavenger) and potassium iodide (KI, a hole (h^+) scavenger) was added to the photodegradation system

of MO aqueous solution in the presence of pure BiFeO₃ and 1.0 mol% Cu-BiFeO₃ nanoparticles. In the obtained results, it can be seen that both KI and IPA have stronger inhibiting effects on the photocatalytic activity of MO aqueous solution than BQ, showing that $OH^•$ and h^+ are the main active species for MO aqueous solution degradation.
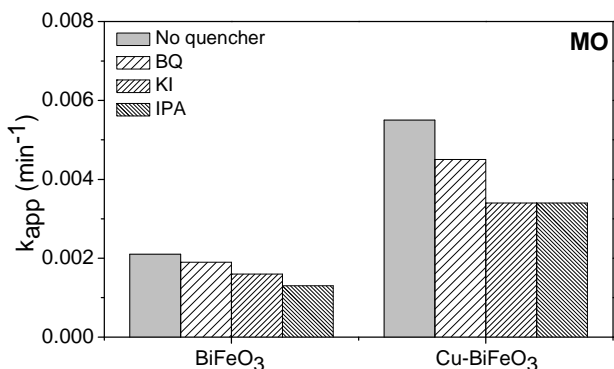
Fig. 7 Kinetic plot of apparent association rate constant, k_{app}, min⁻¹ over pure BiFeO₃ and 1.0 mol% Cu-BiFeO₃ nanoparticles with different quenchers for MO degradation.

The photocatalytic mechanism for MO aqueous solution degradation of 1.0 mol% Cu-BiFeO₃ under visible light irradiation was studied as shown in Fig. 8. The band edge positions of conduction band (CB) potential of semiconductor can be calculated by the following equation: $E_{CB} = x-E^C-0.5E_g$, where x is the absolute electronegativity of the semiconductor, expressed as the geometric mean of the absolute electronegativity of the constituent, which is defined as the arithmetic mean of the atomic electron affinity and the first ionization energy (for BiFeO₃, x is 5.93 eV [32]). E^C is the energy of free electrons on the hydrogen scale (~4.5 eV). E_g is the band gap of the semiconductor. The valence band (VB) of BiFeO₃ can be determined by the following equation: $E_{VB} = E_{CB}+E_g$. The band gap energies of BiFeO₃ (2.14 eV) were obtained from UV-vis DRS results. The conduction band (CB) and valence band (VB) of BiFeO₄ were calculated to be 0.36 and 2.50 eV, respectively. The possible photocatalytic mechanism for MO aqueous solution degradation of 1.0 mol% Cu-BiFeO₃ sample under visible light irradiation was studied. When the semiconductor photocatalyst is irradiated by visible
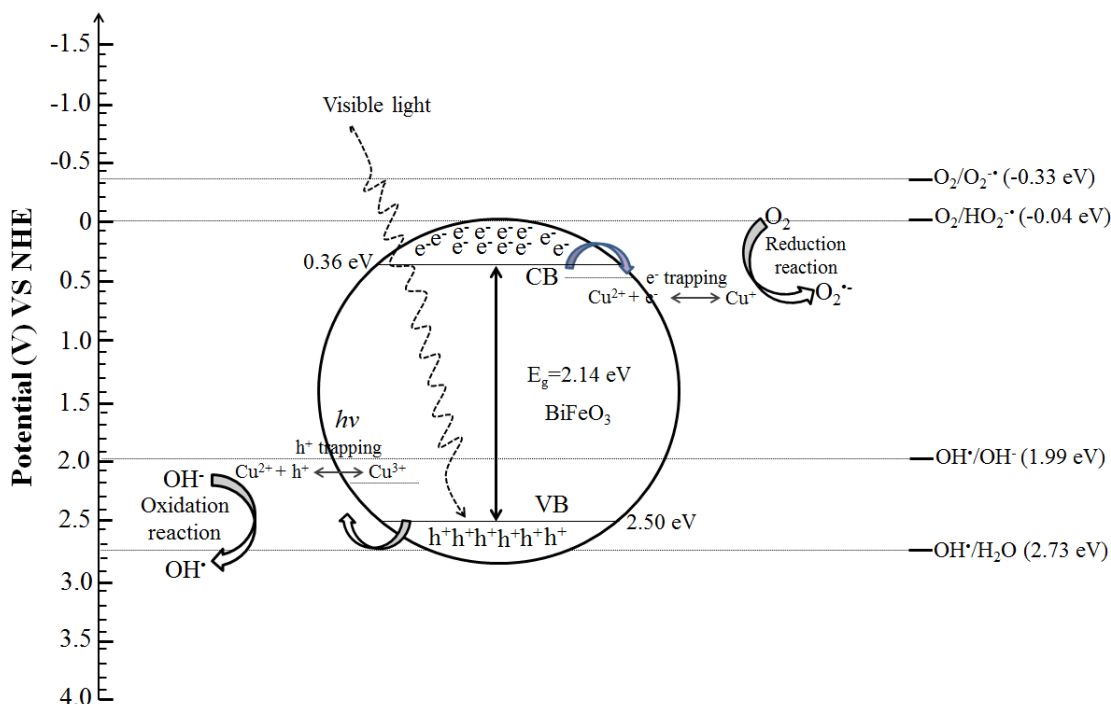
Fig. 8 Photocatalytic mechanism of 1.0 mol% Cu-BiFeO₃ nanoparticles for MO aqueous solution degradation under visible light irradiation.

light, the electrons on valence band (VB) of BiFeO$_3$ could be excited to the conduction band (CB) with simultaneous generation of holes in the valence band. In addition, the photogenerated electrons on the conduction band of BiFeO$_3$ could transfer to Cu^{2+}, resulting in the electrons being trapped by Cu^{2+} ions. However, the electrons on the CB of BiFeO$_3$ and Cu could not then react with molecular oxygen absorbed on the surface of photocatalyst due to the CB potential being lower than the standard redox potential. The photogenerated holes on the BiFeO$_3$ could trap hydroxide ion molecules to finally form hydroxyl radicals. These hydroxyl radicals (OH$^{\bullet}$) are strong oxidizing agents and can completely degrade MO molecules. Moreover, the photogenerated electrons and holes are able to be separated into trap states in the doped material. The presence of Cu^{2+} can act as electron trap (from Cu^{2+} to Cu^{+}) to facilitate the separation of charge carriers by trapping at energy levels close to the conduction or valence bands, respectively [31]. Therefore, Cu^{2+} doping could inhibit the recombination of electron-hole pairs, and therefore enhancing the photocatalytic performance.

3.8 Photoluminescence

The Photoluminescence (PL) technique was helpful to understand the separation and recombination processes of photogenerated charge carriers in BiFeO$_3$ and 1.0 mol% Cu-BiFeO$_3$ nanoparticles, as illustrated in Fig. 9. The PL spectra of all samples excited 345 nm. In Fig. 9a, it can be obviously seen that the PL emission intensity of pure BiFeO$_3$ shows stronger emission. Whereas the PL emission intensity of 1.0 mol% Cu-BiFeO$_3$ shows lower intensity than pure BiFeO$_3$, suggesting that the decrease in recombination rate of electron-hole pairs. In conclusion, the Cu doping into BiFeO$_3$ nanoparticles is beneficial to reduce the recombination rate of photoinduced charge carriers and increase the long-time separation of charge carriers, and then enhance the photocatalytic activity [27]. In order to further confirm the OH$^{\bullet}$ productions on the
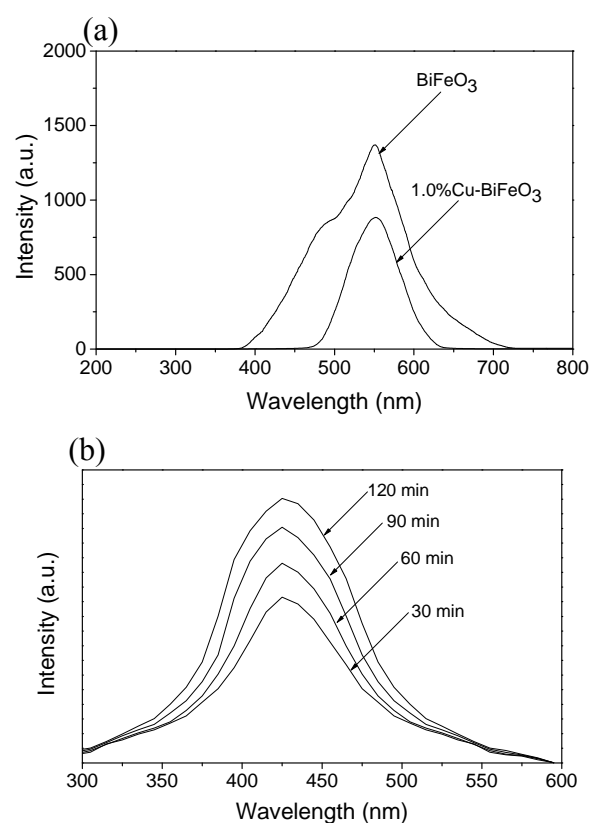
Fig. 9 (a) Photoluminescence (PL) spectra of pure BiFeO$_3$ and 1.0 mol% Cu-BiFeO$_3$ nanoparticles; (b) fluorescent 2-hydroxy terephthalate (TA OH$^{\bullet}$) generated by 1.0 mol% Cu-BiFeO$_3$ under visible light irradiation.

surface of 1.0 mol% Cu-BiFeO$_3$, the sample was detected through the reaction of terephthalic acid (TA) with OH$^{\bullet}$. This forms a fluorescent 2-hydroxy terephthalate (TA-OH$^{\bullet}$) which can be investigated by using fluorescence spectroscopy. The PL intensity of fluorescent 2-hydroxy terephthalate (TA-OH$^{\bullet}$) appeared at 425 nm, it was found that the fluorescence spectra slightly increased with an increase of irradiation time as shown in Fig. 9b.

4. Conclusion

The Cu-BiFeO$_3$ nanoparticle photocatalysts were successfully prepared by a homogeneous precipitation process. The photocatalytic activity of the Cu-BiFeO$_3$ nanoparticle photocatalysts was significantly improved compared to pure BiFeO$_3$. The proper Cu concentration in Cu-BiFeO$_3$ was found to be 1.0 mol%, which

showed the highest photocatalytic activity for degrading MO aqueous solution under visible light irradiation. The enhanced photocatalytic performance of the Cu-BiFeO$_3$ may be attributed to Cu ions acting as a good electron and hole traps at the interface of BiFeO$_3$, which facilitated the separation of charge carriers and reduced the recombination of photogenerated charge carriers. The active species trapping experiments reveals that the hydroxyl radicals (OH$^\bullet$) and holes (h$^+$) played key roles in the degradation of MO aqueous solution under visible light.

Acknowledgements

References

[1]   V. Scuderi, G. Impellizzeri, L. Romano, M. Scuderi, G. Nicotra, K. Bergum, A. Irrera, B. G. Svensson and V. Privitera, TiO2-coated nanostructures for dye photo-degradation in water, *Nanoscale Research Letters* 4 (2014) 458-465.

[2]   W. Yin, W. Wang, L. Zhou, S. Sun and L. Zhang, CTAB-assisted synthesis of monoclinic BiVO$_4$ photocatalyst and its highly efficient degradation of organic dye under visible-light irradiation, *Journal of Hazardous Materials* 173 (2010) 194-199.

[3]   L. Ai, H. Huang, Z. Chen, X. Wei and J. Jiang, Activated carbon/CoFe$_2$O$_4$ composites: Facile synthesis, magnetic performance and their potential application for the removal of malachite green from water, *Chemical Engineering Journal* 156 (2010) 243-249.

[4]   M. Behera and G. Giri, Inquiring the photocatalytic activity of cuprous oxide nanoparticles synthesized by a green route on methylene blue dye, *International Journal of Indian Chemical* 7 (2016) 157-166.

[5]   F. Duan, Q. Zhang, D. Shia and M. Chen, Enhanced visible light photocatalytic activity of Bi$_2$WO$_6$ via modification with polypyrrole, *Applied Surface Science* 268 (2013) 129-135.

[6]   C. Yu, K. Yang, J. C. Yu, F. Cao, X. Li and X. Zhou, Fast fabrication of CO$_3$O$_4$ and CuO/BiVO$_4$ composite photocatalysts with high crystallinity and enhanced photocatalytic activity via ultrasound irradiation, *Journal of Alloys and Compounds* 509 (2011) 4547-4552.

[7]   T. Guo-Qiang, Z. Yu-Qin, M. Hong-Yan, X. Ao and R. Hui-Jun, Controllable microwave hydrothermal synthesis of bismuth ferrites and photocatalytic characterization, *Journal of the American Ceramic Society* 95 (2012) 280-289.

[8]   Y. Huo, Y. Jin and Y. Zhang, Citric acid assisted solvothermal synthesis of BiFeO$_3$ microspheres with high visible-light photocatalytic activity, *Journal of Molecular Catalysis A: Chemical* 331 (2010) 15-20.

[9]   T. Xian, H. Yang, J. F. Dai, Z. Q. Wei and W. J. Feng, Photocatalytic properties of BiFeO$_3$ nanoparticles with different sizes, *Materials Letters* 65 (2011) 1573-1575.

[10]   Y. Liu, R. Zuo and S. Qi, Controllable preparation of BiFeO3@carbon core/shell nanofibers with enhanced visible photocatalytic activity, *Journal of Molecular Catalysis A: Chemical* 376 (2013) 1-6.

[11]   R. Guo, L. Fang, W. Dong, F. Zheng and M. Shen, Enhanced Photocatalytic activity and ferromagnetism in Gd doped BiFeO3 nanoparticles, *Journal of Physical. Chemistry C* 114 (2010) 21390-21396.

[12]   L. J. Di, H. Yang, G. Hu, T. Xian, J. Y. Ma, J. L. Jiang, R. S. Li and Z. Q. Wei, Enhanced photocatalytic activity of BiFeO3 particles by surface decoration with Ag nanoparticles, *Journal of Materials Science: Materials in Electronics* 25 (2014) 2463-2469.

[13]   M. Arora and M. Kumar, Electron spin resonance probed enhanced magnetization and optical properties of Sm-doped BiFeO$_3$ nanoparticles, *Materials Letters* 137 (2014) 285-288.

[14]   F. Niu, D. Chen, L. Qin, T. Gao, N. Zhang, S. Wang, Z. Chen, J. Y. Wang, X. Sun and Y. Huang, Synthesis of Pt/BiFeO$_3$ heterostructured photocatalysts for highly efficient visible-light photocatalytic performances, *Solar Energy Materials & Solar Cells* 143 (2015) 386-396.

[15]   R. Dhanalakshmi, M. Muneeswaran, K. Shalini and N. V. Giridharan, Enhanced photocatalytic activity of La-substituted BiFeO$_3$ nanostructures on the degradation of phenol red, *Materials Letters* 165 (2016) 205-209.

[16]   Y. N. Feng, H. C. Wang, Y. Shen, Y. H. Lin and C. W. Nan, Magnetic and photocatalytic behaviors of Ba-doped BiFeO3 nanofibers, *International Journal of Applied Ceramic Technology* 11 (2014) 676-680.

[17]   R. R. Bacsa and J. Kiwi, Effect of rutile phase on the photocatalytic properties of nanocrystalline Titania during the degradation of p-coumaric acid, *Applied Catalysis B: Environmental* 16 (1998) 19-29.

[18]   H. Li, G. Liu and X. Duan, Monoclinic BiVO$_4$ with regular morphologies: hydrothermal synthesis, characterization and photocatalytic properties, *Materials Chemistry and Physics* 115 (2009) 9-13.

[19] S. Liu and J. Yu, Cooperative self-construction and enhanced optical absorption of nanoplates-assembled hierarchical Bi_2WO_6 flowers, *Journal of Solid State Chemistry* 181 (2008) 1048-1055.

[20] M. Wang, Q. Liu, Y. Che, L. Zhang and D. Zhang, Characterization and photocatalytic properties of N-doped $BiVO_4$ synthesized via a sol–gel method, *Journal of Alloys and Compounds* 548 (2013) 70-76.

[21] X. Wang, Y. Lin, X. Ding and J. Jiang, Enhanced visible-light-response photocatalytic activity of bismuth ferrite nanoparticles, *Journal of Alloys and Compounds* 509 (2011) 6585-6588.

[22] S. Guo, X. Li, H. Wang, F. Dong and Z. Wu, Fe-ions modified mesoporous Bi_2WO_6 nanosheets with high visible light photocatalytic activity, *Journal of Colloid and Interface Science* 369 (2012) 373-380.

[23] W. P. Wang, H. Yang, T. Xian and J. L. Jiang, Properties of $CoFe_2O_4$ Nanoparticles Synthesized by a Polyacrylamide Gel Route, *Materials Transactions* 53 (2012) 1586-1589.

[24] A. P. Grosvenor, B. A. Kobe, M. C. Biesinger and N. S. McIntyre, Investigation of multiplet splitting of Fe 2p XPS spectra and bonding in iron compounds, *Surface and Interface Analysis* 36 (2004) 1564-1574.

[25] S. Chala, K. Wetchakun, S. Phanichphant, B. Inceesungvorn and N. Wetchakun, Enhanced visible-light-response photocatalytic degradation of methylene blue on Fe-loaded $BiVO_4$ photocatalyst, *Journal of Alloys and Compounds* 597 (2014) 129-135.

[26] S. Sriwichai, H. Ranwongsa, K. Wetchakun, S. Phanichphant and N. Wetchakun, Effect of iron loading on the photocatalytic performance of Bi_2WO_6 photocatalyst, *Superlattices and Microstructures* 76 (2014) 362-375.

[27] S. Chaiwichian, K. Wetchakun, S. Phanichphant, W. Kangwansupamonkon and N. Wetchakun, Effect of iron doping on the photocatalytic activities of $Bi_2WO_6/BiVO_4$ composites, *RSC Advances* 6 (2016) 54060-54068.

[28] H. Yuan, J. Liu, J. Li, Y. Li, X. Wang, Y. Zhang, J. Jiang, S. Chen, C. Zhao and D. Qian, Designed synthesis of a novel $BiVO_4$–Cu_2O–TiO_2 as an efficient visible-light-responding photocatalyst, *Journal of Colloid and Interface Science* 444 (2015) 58-66.

[29] H. Xu, H. Li, C. Wu, J. Chu, Y. Yan, H. Shu and Z. Gu, Preparation, characterization and photocatalytic properties of Cu-loaded $BiVO_4$, *Journal of Hazardous Materials* 153 (2008) 877-884.

[30] S. Min, F. Wang, Z. Jin and J. Xu, Cu_2O nanoparticles decorated $BiVO_4$ as an effective visible-light-driven p-n heterojunction photocatalyst for methylene blue degradation, *Superlattices and Microstructures* 74 (2014) 294-307.

[31] G. Tann, J. Huang, L. Zhang, H. Ren and A. Xia, An enhanced visible-light-driven photocatalyst: Conduction band control of Bi_2WO_6 crystallites by Cu ion modification, *Ceramics International* 40 (2014) 11671-11679.

[32] J. F. Dai, T. Xian, L. J. Di and H. Yang, Preparation of BiFeO3-Graphene nanocomposites and their enhanced photocatalytic activities, *Journal of Nanomaterials* 5 (2013) 642897-642902.